Marine and Petroleum Geology 105 (2019) 222–237

Contents lists available at ScienceDirect

Marine and Petroleum Geology

journal homepage: www.elsevier.com/locate/marpetgeo

Research paper

Fault-related fracture modeling in the complex tectonic environment of the Malay Basin, offshore Malaysia: An integrated 4D geomechanical approach

Laurent Maerten[a,*], Xavier Legrand[b], Claire Castagnac[c], Marie Lefranc[d], Jean-Pierre Joonnekindt[a], Frantz Maerten[e]

[a] Schlumberger Montpellier, France
[b] PETRONAS, Malaysia
[c] Schlumberger Aachen, Germany
[d] Schlumberger Boston, USA
[e] YouWol Montpellier, France

ARTICLE INFO

Keywords:
Fractured reservoirs
Malay basin
Geomechanics
Restoration
Stress inversion
Stress modeling

ABSTRACT

In the South-East prong of Eurasia prevails a positive tectonic inversion, where the Malay Basin and its complex oil and gas reservoirs were formed. Therefore, the characterization of the natural fracture network originated from the complex multi-tectonic events of this area remains challenging. This contribution presents a 4D innovative approach for improving the geomechanics-based assessment of fault-related fractures in such exigent environment. The workflow consists of several steps to reduce uncertainties in the fractured reservoir modeling, both in estimating (i) the paleo-geometry of the main structures using 3D reconstruction techniques and (ii), the paleo-tectonic stresses using fracture-based stress inversion technology, both steps being essential to comprehensive geomechanical simulations through geological time.

This acute fractured reservoir characterization workflow was therefore applied in a field development plan in the Malay Basin, offshore Malaysia. Well data analysis, refined seismic interpretations, 2D/3D structural restorations and paleo-stress inversions were integrated to manage uncertainties in the discrete fracture simulation. The model reveals evidences of two successive tectonic events: a Paleogene extension with a normal-slip fault regime (σ_H = > N66°) and a Neogene contraction with a strike-slip fault regime (σ_H = > N174°). This tectonic inversion is associated with a redirection of the far field stress, as well asthe location and orientation of the natural fracture network during its growth. The proposed workflow improves the understanding of the fractured reservoir characterization greatly and is of help to appraise future development plans better.

1. Introduction

In the Malay Basin reservoirs, the natural fractures are mostly below the resolution of the seismic reflection data. Such natural fractures are known to be of importance both to constrain the hydrocarbon flow and cause in severe wellbore instability issues. Therefore, it is of interest to understand and to quantify the spatial and temporal development of these natural fractures as well as their dynamic, kinematic and geometric properties (Narr et al., 2006). Indeed, in Geosciences (exploration and production of the petroleum Industry), minimizing the uncertainty of the natural fracture assessment has great economic impact and impacts decision making. Acquiring this information would assist both in the understanding of trapping location and in the optimization of well trajectories to target and/or to avoid the natural fracture zones. To address these economic issues, methods of reservoir fracture modeling have been developed over the last decades.

The curvature analysis methods, intensively utilized in the industry are useful for estimating fracture orientations and clustering of bent or folded strata (Murray, 1968; Thomas et al., 1974; Lisle, 1994; Fischer and Wilkerson, 2000; Hennings et al., 2000). However, some authors are not confident with the predictive capability (Schultz-Ela and Yeh, 1992; Gibbs et al., 1997; Jamison, 1997) because the effects of faulting and layer thickness are ignored, and curvature considers only the present-day geometry, and not the kinematic evolution. Furthermore, the technique is too sensitive to seismic reflection data acquisition and processing.

The statistical methods, for instance based on the fault power-law size distribution (Childs et al., 1990; Walsh and Watterson, 1991; Sassi

* Corresponding author.
E-mail address: lmaerten@slb.com (L. Maerten).

https://doi.org/10.1016/j.marpetgeo.2019.04.025
Received 19 November 2018; Received in revised form 6 April 2019; Accepted 18 April 2019
Available online 24 April 2019

et al., 1992; Yielding et al., 1992; Schlische et al., 1996), on the stochastic clustering process (Munthe et al., 1993; Damsleth et al., 1998) or on the theoretical fractal nature of fracturing (Gauthier and Lake, 1993), are also used to model fractures in reservoirs. Although the size distributions are predictable, fracture mechanics is not considered and hence orientation and location of the fractures are not always reliable.

Pioneer work by Hudson (1981) has shown a possible detection of fracture networks through seismic attribute processing (Schoenberg and Sayers, 1995; Neves et al., 2004), which illuminate features within the original seismic data that correlate with faulting and fracture corridors. More recently, diffracting imaging (Moser and Howard, 2008) has been used to identify local heterogeneities and discontinuities in the subsurface (Sturzu et al., 2015). However, despite the tremendous detail now available from 3D seismic reflection techniques and the recent advance in seismic attribute processing, most of the natural fractures cannot be detected at the current resolution of the seismic reflection data.

Recently, structure restoration methods, used by structural geologists to check the consistency of the subsurface structural interpretations, have been extended to predict areas that have undergone large strains and to relate the strains to structural heterogeneities such as faults and joints (Hennings et al., 2000; Sanders et al., 2002, 2004; Kloppenburg et al., 2003). Nonetheless, as for the previous techniques to model fractures, geometric restoration does not consider rock deformation as a physical phenomenon. Maerten and Maerten (2006) and Stockmeyer et al. (2018) have demonstrated that adding mechanics to structural restoration could help model natural fractures in reservoirs for some configurations only as these new techniques are too dependent on unphysical boundary conditions (Lovely et al., 2012).

Numerical models of rock deformation based on continuum mechanics are becoming industry standard in providing efficient means for modeling natural fractures in reservoirs, where there is a clear relationship between the natural fracture system and larger scale structures. Over the past two decades, pioneer studies (Maerten, 1999, 2010; Bourne and Willemse, 2001; Maerten et al., 2002) have proven that adding a geomechanical rationale to stochastic techniques improves their predictive capability and leads to more realistic fractured reservoir models. The basic methodology consists of calculating the stress distribution at the time of fracturing using the available reservoir structure data such as faults, fractures and folds, the rock type and the tectonic setting that can be characterized by stress or strain magnitude and orientation. Then, the calculated stress fields, perturbed by the main structures, combined with rock failure criteria are used to model natural fracture networks (i.e. orientation, location, and spatial density). Although this method has been successfully applied to modeling fractures in naturally fractured reservoirs (Bourne et al., 2000; Maerten et al., 2006; Dee et al., 2007; Phillips et al., 2014), it turns out to be difficult to apply to areas, as in the Malay Basin, where the structural evolution over time is complex and severe and where natural fault-related fractures were developed during several successive tectonic events.

In this contribution, we use the assumption, corroborated by others (Legrand et al., 2013; Lefranc et al., 2014), that most of the observed natural fractures in the study area of the Malay Basin, are fault-related fractures and that other mechanisms such as bending, stratigraphy mechanical contrast, compaction and diagenesis are secondary. Therefore, no attempts were made to consider such mechanisms even though they probably contribute to a smaller part of the observed natural fractures. We have therefore developed and applied an integrated 4D geomechanical approach to model fault-related fracture distribution in reservoirs of the Malay Basin. The basic methodology consists of calculating the stress distribution at the time of fracturing using the paleo reservoir structure data such as faults, fractures and folds, obtained from 3D restoration, the rock type and the tectonic setting that can be characterized by stress or strain magnitude and orientation. Then, the calculated stress fields, perturbed by the main structures, combined with rock failure criteria are used to model natural fracture networks, *i.e.* orientation, location, and spatial density.

2. Geological settings

2.1. Regional tectonics

Commonly, petroleum systems associated with Cenozoic deltaic systems developed in a passive margin environment, therefore they have been experiencing gravity-related deformation only e.g., Nigeria, Congo, Angola, Gulf of Mexico and Brazil and hence do not exhibit strong evidence of tectonic deformation. These petroleum systems do not generally exhibit any evidence of tectonic deformation. Conversely, Southeast Asia present-day stresses can be modeled only by considering the plate boundary forces affecting the region, *i.e.* a northeastward displacement of the Australian plate associated with the subduction of Sumatra-Java and a westward displacement of the West Pacific plate associated with the subduction of Philippines. Numerous existing models suggest a complex tectonic history of this basin. The Malay Basin, located East offshore of the South-East prong of Eurasia, known as Malaysian Peninsula along the west border of Sundaland, has been interpreted as a rifting combined either with wrench faulting (Hamilton, 1979) or with a mantle plume (Hutchison, 1989), being in a back-arc basin, existing behind the Sumatra-Java arc (e.g. Kingston et al., 1983). Other causes of this basin formation in response to extension are dextral shear along inherited NW-striking faults (Polachan and Sattayarak, 1989), pull-apart basins that accommodated oroclinal bending of Sundaland (Hutchison, 1992, 2009; Zahirovic et al., 2014), rotating stress field related to the Indo-Eurasian collision (Huchon et al., 1994). The most complete interpretation refers to the extrusion model (Tapponnier et al., 1982) and is summarized as follows. The two subduction zones (Sumatra-Java and Philippines) respectively bound the South and the East of the Eurasian plate animated by a southeastward displacement to form the Sunda continental prong surrounded by some of the most active faults on the planet. In the south-western part, the Malay Basin is bounded by a strike-slip fault thought to be a branch of a southeast-trending crustal shear band that coincides with the western edge of Sundaland (Fig. 1). It was formed as an early result of deformation driven by the Indian plate collision with the Asian plate. Associated with an inherent shear and rotation (England and Molnard, 1990), a kinematics of extension and inversion invokes a distributed left-lateral shear for the development of the Malay Basin, offshore Peninsular of Malaysia (Madon, 1995; Mansor et al., 2014).

2.2. The Malay Basin

The Malay Basin is an elongated basin of 400 km in length and of 200 km in width, filled by continental to marine clastic sediments since early Oligocene and was developed through structural changes consistent with a multi-phased extrusion model and displacements in which India has successively pushed Sundaland (Tapponnier et al., 1986). Initially, the extrusion imparted sinistral transtensional wrenching on the axial basement fault along the basin length. In early Miocene, an important coupling of the Eurasian plate with the Australian and Pacific plates led to a compressional stress known as the pervasive tectonic inversion in Sundaland (Hall and Morley, 2004; Doust and Sumner, 2007). Thought to be the consequence of an incipient continental collision of NW shelf of Australia against Timor Island at the southern end of Maritime Southeast Asia, these forces drive a structural inversion accompanied by wrench slip reversal producing transpression. At present day, this complex tectonic confers to the basin an inverted geometry as shown in Fig. 2.

The Oligocene sedimentation, which is generally terrestrial deposits with minor marine influence, recorded the major extension tectonics and the subsidence. It comprises the principal source rock of the Malay Basin. This early period of extensional tectonics in the basin had given

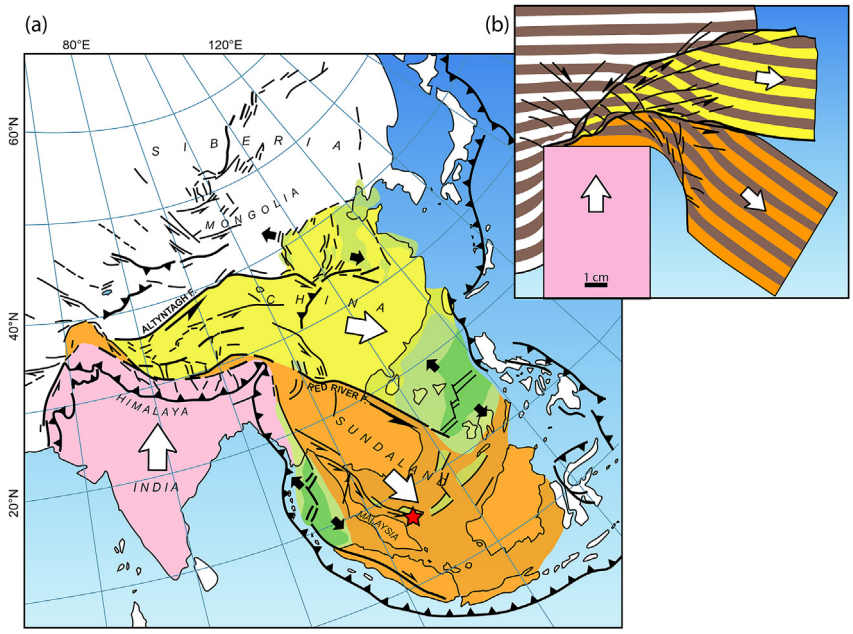

Fig. 1. Southeastern Asian Tectonics. (a) Structural map of southern Asia. The red star locates the study area. (b). Deformation model of southern Asia (figure modified from Tapponnier et al., 1982). (For interpretation of the references to color in this figure legend, the reader is referred to the Web version of this article.)

rise to the formation of a series of grabens/half-grabens and horst blocks, which in certain areas formed large scale depressions providing the physiographic lows for lake development. From Oligocene to early Miocene, three major depositional environment subdivisions, *i.e.* lake, lakeshore and lacustrine plain are defined for the sediments and record a succession of alternating sand-dominated and shale-dominated, fluvio-lacustrine sequences. These deposits, known as a succession of Group in order of decreasing age from M up to K, show increasing lacustrine influence towards the center of the basin (Fig. 3).

With the onset of the lower Miocene, rifting declined, and thermal sagging came to dominate throughout the Neogene. This resulted in broadening of the subsiding area and increasing marine influence.

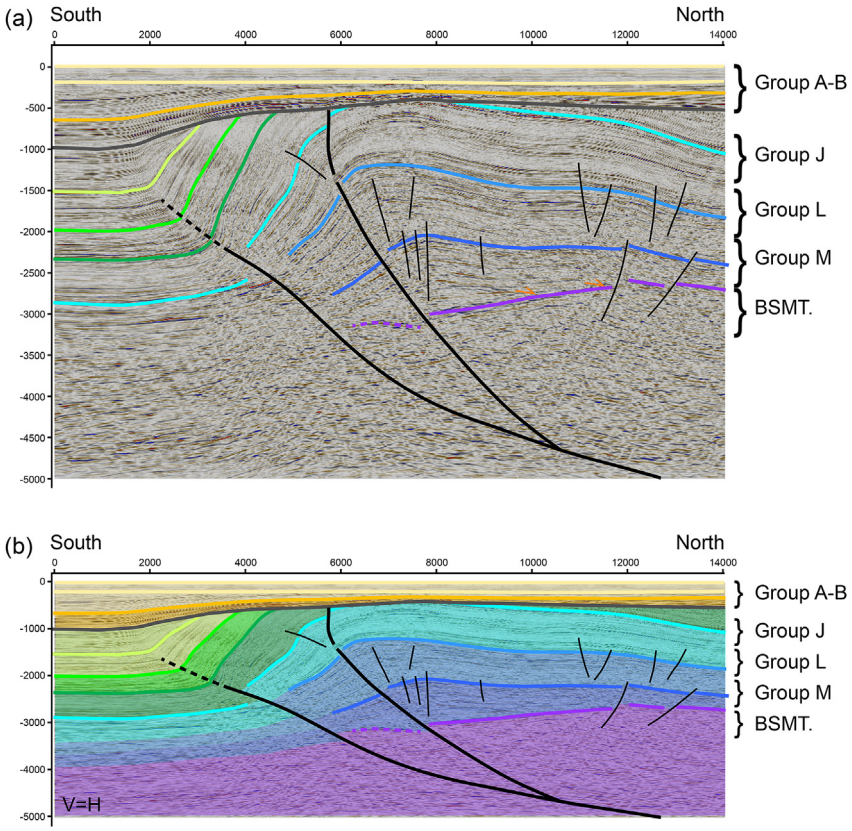

Fig. 2. Depth converted cross-section of the inverted Malay Basin. (a) 2D seismic reflection and interpretation (V = 1.75H). (b) 2D structural model (V=H). See stratigraphic column of Fig. 3 for geologic age reference.

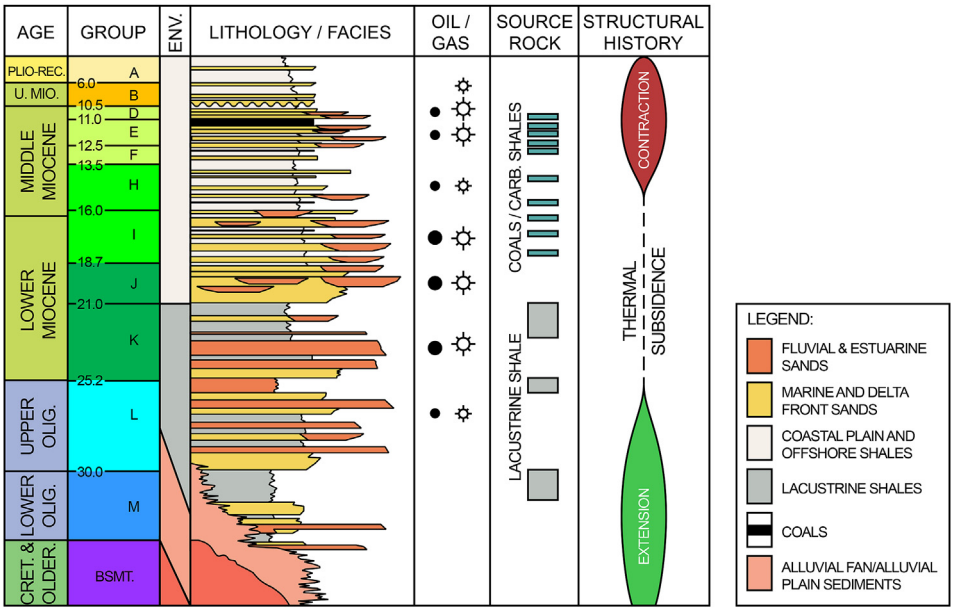

Fig. 3. Regional stratigraphy and hydrocarbon occurrences of the Malay Basin (adapted from EPIC, 1994 and PETRONAS, 1999).

Sedimentation during the Miocene was accompanied by structural inversions that caused major east-trending anticlines to grow in the axial part of the basin (Fig. 2). The anticlines are known to be the result of right-lateral wrench deformation (Hamilton, 1979; Madon, 1997). The Miocene to recent sediments, which are coastal plain to shallow marine and known as a succession of Group in order of decreasing age from J up to A, experienced a succession of compressive tectonic pulses and represent the main reservoirs (Madon, 1995). The best reservoirs are observed to occur in the coastal environments and to a lesser degree in lower coastal plain environment (Fig. 3). However, good quality source rocks are found to be concentrated in lower coastal plain environment and to a certain extent in coastal fluvio-marine environment. Therefore, deltaic and shallow marine siliciclastic prevail in the Neogene succession of the basin.

In such complex geological context, the succession of tectonic events, subsidence, uplift and erosion, confers to the reservoir rocks a singular fracture network, which is very challenging to characterize, especially when one recognizes that these fractures are known to be the origin of both significantly altering the flow of hydrocarbons and potentially result in severe wellbore instability problems. In the Malay Basin reservoirs, it is therefore important to understand and quantify the spatial and temporal development of these fractures as well as their properties e.g., geometry, throw, aperture, permeability, etc … Indeed, natural fractures, analyzed along three wells, show three main trends (Fig. 4) that are not systematically observed along each well, suggesting several fracture sets that are not all present at these three locations or lesser fracture sets but with varying orientation spatially.

3. Method

In this contribution we consider that most of these fractures are faults-related fractures and that subsequent folding or other fracture mechanisms did not affect the global fracturing processes significantly. It is also important to note that the assumption that fractures are related to reservoir structures such as faults and folds, cannot be generalized. Indeed, fractures development may predate or postdate the structure formation and larger scale stress perturbations may not have any associated fracture arrays. The proposed method solely focuses on the case where faulting is driving stress perturbations that would affect secondary fracture growth. To compute the heterogeneous stress around active faults and thereby model the faults-related fracture orientation and intensity trends geomechanical simulations have been carried out.

3.1. Vocabulary and symbols

The term “fault” is used for the seismically observed faults. The small-scale faults observed along the wells or modeled will be called “shear fractures”. Furthermore, to prevent from any confusion between the geological inversion and the paleo-stress inversion used in the study, the geological inversion will be written with a capital **I** as “Inversion phase” and the process for inverting the paleo-stress will be

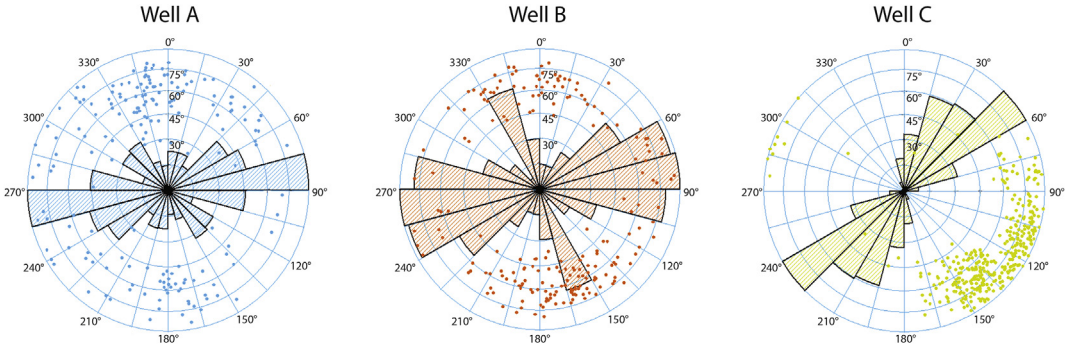

Fig. 4. Rose diagrams showing fracture characteristics (dip azimuth with dip angle and strike presentation) per well.

written with a lower case as “paleo-stress inversion”.

The proposed method used the three mechanical fracture types that are described as follow. These fracture types are based on their development mechanism and their relationship with the orientations of the three principal stresses.

Opening mode fractures form when the effective tensile stress in a direction perpendicular to the potential fracture plane reaches the tensile strength of the rock. Opening mode fractures show an extension perpendicular to each fracture wall. The most common opening mode fractures are the joints but veins (tension gashes) and dikes are also included (Pollard and Aydin, 1988). Opening mode fractures form in the plane perpendicular to the least compressive principal stress direction, $\vec{\sigma_3}$.

Closing mode fractures or anti-cracks (Fletcher and Pollard, 1981) form with a compressive stress in a direction perpendicular to the potential fracture plane. Closing mode fractures show a contraction perpendicular to each fracture wall. In clastic rocks at reservoir conditions, the most typical closing mode fractures are compaction bands (Mollema and Antonellini, 1996; Aydin et al., 2006). Closing mode fractures will form in a plane perpendicular to the most compressive principal stress direction, $\vec{\sigma_1}$.

Shearing mode fractures are generated by shear stress. A shearing mode fracture is a fracture along which the relative movement is parallel to each fracture wall. The most common kind of shearing mode fractures are faults and shear deformation bands (Aydin, 1978; Aydin et al., 2006). A shearing mode fracture is one of the two conjugate planes, oriented at acute angles δ on either side of the most compressive principal stress direction, $\vec{\sigma_1}$, and with opposite sense of shear direction. δ is defined according to the Coulomb criterion such that:

$$\delta = \frac{\pi}{4} - \frac{\varphi}{2}, \tag{1}$$

where ϕ is the angle of rock internal friction. We consider here the conjugate shearing mode based on Anderson’s (1905) application of the Mohr-Coulomb failure criterion, which assumes that shearing mode fractures form parallel to the intermediate principal stress direction, $\vec{\sigma_2}$.

To facilitate the reading, Table 1 defines all symbols used in this contribution.

3.2. Geomechanical simulation

Three key elements are essential for modeling natural fracture network characteristics using geomechanical simulations. The first key element is the geological model, referred to the geometry of the subsurface geology. It is the most important element in geomechanical simulation, even though it is recurrently neglected because geological models are often oversimplified for technical and/or practical reasons. Geological models should resemble past and/or present-day natural structures as close as possible. This includes for instance sedimentary layers, faults and fractures, folds or any geological objects. Commonly, a model of present day observed geological structures can be used as a proxy for the past geometry. This is particularly true in normal faulting areas, where the local extension does not exceed 10–20%. However, for highly deformed areas such as in the Malay Basin, present day geometry cannot be used to model past deformation. The second key element is the tectonic stress, which is referring to the type (normal, strike-slip or reverse), orientation (*i.e.* σ_H) and relative magnitude of the regional or local tectonic stresses through geological time. This important element of the geomechanical modeling is the most difficult to control. While there are techniques for measuring some components of the present-day tectonic stress, it becomes tricky to measure past tectonic stresses. Due to the complexity of the geodynamic setting of Sundaland, a series of tectonic events occurred, causing the Malay basin development. Therefore, tectonic stresses always have been partly interpreted introducing uncertainties. Finally, the third key element is the rock properties and mechanical behavior. This element of the geomechanical modeling is the least uncertain to estimate. Thanks to laboratory testing we have a fair understanding of rock properties and behavior. These can be extrapolated using burial history and known rules on how the rocks evolve over time, *e.g.* compaction and porosity.

Consequently, an efficient geomechanics-based natural fracture modeling for the Malay Basin case study requires to address two central issues: (i) how can we minimize uncertainties while estimating the 3D paleo-geometry of the structures over time? and (ii), how can we minimize uncertainties while assessing the paleo-tectonic stresses used as boundary conditions in the geomechanical simulations?

Table 1
Symbol definitions.

Symbol	Comments
Fault properties	
μ	Sliding friction
Rock properties	
ν	Poisson's ratio
E	Young's modulus
ϕ	Friction angle
Stress	
$\sigma_1 \geq \sigma_2 \geq \sigma_3$	Principal effective stress magnitudes (positive compression)
σ_v	Magnitude of the far field vertical stress
σ_H	Magnitude of the far field maximum horizontal stress
σ_h	Magnitude of the far field minimum horizontal stress
θ	Orientation of σ_H defined clockwise from the North
S_0	Maximum Coulomb shear stress
σ_m	Mean stress
τ_m	Shear stress
R	Stress ratio $R = (\sigma_2\text{-}\sigma_3)/(\sigma_1\text{-}\sigma_3)$
$\bar{R}$	Stress ratio defined by Lejri et al. (2015) for Andersonian regimes
Acronyms	
BEM	Boundary Element Method
FEM	Finite Element Method
DFN	Discrete Fracture Network

3.3. General workflow

To overcome these challenging fracture characterization and modeling issues in the Malay Basin, we have developed a 4D approach that is mainly based on geomechanical simulations. The method consists on a workflow (Fig. 5) comprising the following main steps: (a) Data collection including interpretation and analysis of the available structural data, (b) 3D model building of the study area honoring the completed data set, (c) 3D geomechanics-based structural restoration to capture the geometry of the structure over time, (d) 3D forward geomechanical modeling to compute heterogeneous stress field around paleo-active faults for each key tectonic event using the paleo-geometry of faults, horizons and observed natural fractures together with inverted regional paleo-stresses as constraints and (e), 3D fracture modeling using failure criteria to simulate fracture properties (type, orientation and distribution) that in turns drive the multiphase Discrete Fracture Network (DFN) models.

3.3.1. Data interpretation and analysis

This first step of the workflow is fundamental in the fracture modeling procedure using the geomechanics as this is where the necessary data is analyzed, interpreted and quality controlled. It also includes the lithology of the geological units and rock properties estimated as these are used to strengthened the seismic-based interpretation and the structural analysis and to constrain the geomechanical simulations.

As in any geomechanical simulation, the geometry of the model is a fundamental parameter. Therefore, mechanical anisotropy surfaces must be honored as much as possible to reflect natural conditions, and then faults and horizons must be interpreted at depth and laterally in extenso. Geological models must not be oversimplified for technical and/or practical reasons and the fault modeling should not be

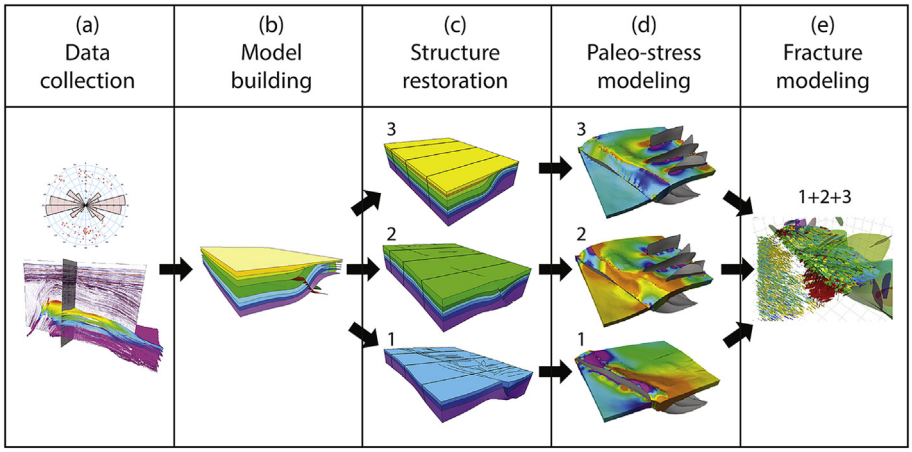

Fig. 5. General workflow of the 4D geomechanical approach. (a) Data collection that mainly includes 3D seismic interpretation and image log analysis, (b) 3D model building of the structural-based interpretation, (c) 3D geomechanically-based restoration to recover the paleo-geometry of the structure for key tectonic events over time, (d) Paleo-stress modeling that includes inverted far field stress and forward stress modeling and (e), Discrete Fracture Network (DFN) modeling.

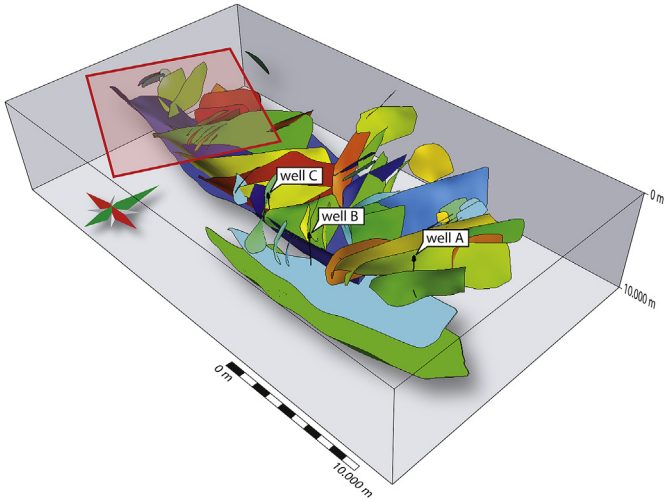

Fig. 6. Fault framework model. The red polygon is the study area. (For interpretation of the references to color in this figure legend, the reader is referred to the Web version of this article.)

restrained to the reservoir unless faults are located only here naturally.

Finally, this step includes the analysis of the seismic scale fault as well asthe analysis of the natural fracture observed from core and image logs. The aim is to appreciate the available data and how it could relate to the tectonic calendar of the area. The three natural fracture types (opening mode, closing mode and shearing mode fractures) are used to classify the observed fractures that will be used in the simulations.

3.3.2. 3D model building

To reduce uncertainty on the geometry of the structure we must preserve the model structural integrity and complexity. Therefore, once the seismic reflection data interpretation is done, the next step consists on building 3D structural model that must honor as much as possible the interpreted geometry (faults and horizons) of the subsurface. This model will be the base of the subsequent modeling steps such as the 3D restoration process, the forward stress simulation around faults and the DFN modeling. When necessary, the 3D model building could be invoked several times to reconstruct the eroded parts of the model that are required for a complete restoration over geological time.

For that purpose, we use a volume-based modeling approach (Lajaunie et al., 1997; Courrioux et al., 2001; Mallet, 2002; Souche et al., 2013). The horizons are defined implicitly inside a tetrahedral mesh covering the volume of interest. This is very different from classical approaches where horizons are defined explicitly by grids or surfaces made of triangles. With an implicit formulation, every single horizon is attached to a value of a scalar attribute named “stratigraphy”, defined on all the nodes of a 3D mesh. The geometry of each horizon is then defined by an iso-surface of the stratigraphy attribute and extracted from the 3D mesh. By interpolating or modifying the values of the stratigraphy attributes within the volume of interest, the geometry of the corresponding horizons can be easily modeled or modified. As the 3D tetrahedral mesh representing the volume of

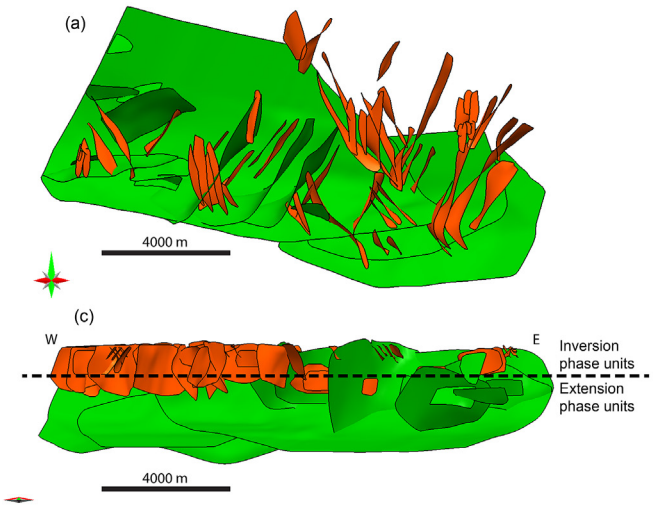

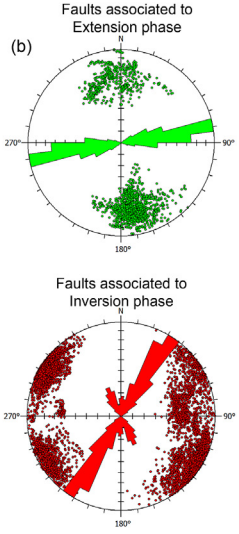

Fig. 7. Fault analysis. (a) Top view of faults initiated with the extension phase (green) versus faults related to the syn-inversion tectonics (orange). (b) Rose diagrams with orientations (dip angle and dip azimuth) of faults associated with both tectonic phases. (c) Side view of the fault model showing that most of the orange faults postdate the extension tectonics. (For interpretation of the references to color in this figure legend, the reader is referred to the Web version of this article.)

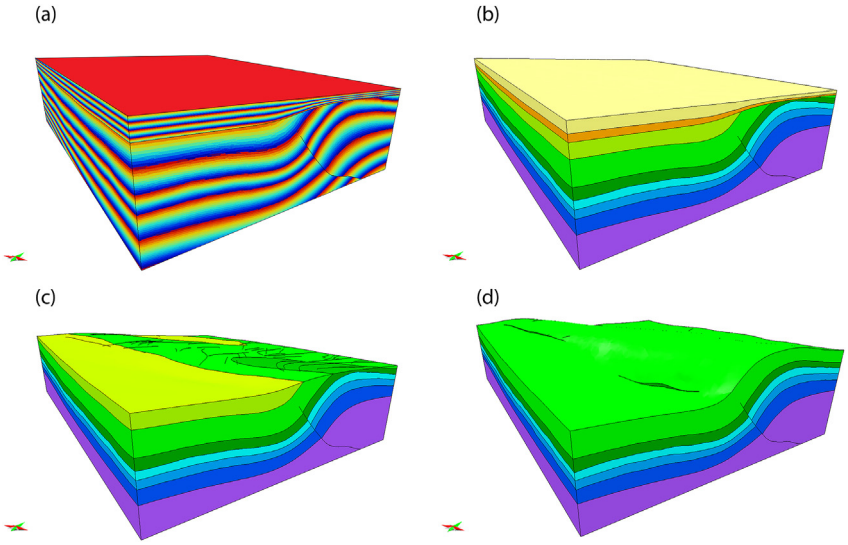

Fig. 8. 3D model building. (a) Stratigraphic attribute computed in the entire model showing fault contacts and two units above and below the unconformity. (b) 3D model with the actual geometry. (c) 3D reconstructed model showing the eroded units at the top. (d) 3D reconstructed model of the eroded units.

interest has internal boundaries (discontinuities) representing faults and unconformities, any iso-surface extracted in this mesh will have naturally perfect contacts along mechanical anisotropy surfaces for instance, faults and unconformities. Therefore, the set of built horizons and the faults define a suitable sealed model.

3.3.3. Subsurface paleo-geometry reconstruction

Once a realistic 3D geological model has been built, a thorough and well constrained 3D restoration of the geological structure must be achieved to obtain a realistic estimate of the structure geometry over geological time. To do it, a numerical tool based on finite element method (FEM), which honors the full complement of physical laws that govern geological deformation so-called Dynel3D has been used. The formulation can accommodate large displacements and strains for a heterogeneous, anisotropic and discontinuous medium. The tool is primarily used for structural restoration (Maerten and Maerten, 2006, 2015; Vidal-Royo et al., 2011; Abul Khair et al., 2013), where physical laws and linear elastic theory replace kinematic and geometric constraints commonly used for restoring geological structures, such as preservation of segment length, surface area and volume (Dahlstrom, 1969; Suppe, 1983). Dynel3D computes the deformation from the restoration of complex geological structures through time. These complex structures include faults, folds, bedding slip, and inhomogeneous mechanical properties. The workflow consists in building a 3D sealed geological model with rock properties, horizons, fault and boundary surfaces and sequentially removing the sedimentary layers one by one and to constrain the top of the next older layer to flatten along a horizontal surface representing the upper surface of the earth. The faults can translate, rotate and deform during the restoration. Because the study area had a long history of subsidence, sedimentation, uplift and erosion, we use decompaction during the restoration process.

3.3.4. Stress modeling

3.3.4.1. Paleo far field stress inversion. The main unknown for geomechanical simulations is the paleo-tectonic stress used as far field stress boundary conditions. Indeed, even though the geologic history of an area is known, it is always difficult to estimate the far field paleo-tectonic stresses in terms of both the orientations and the magnitudes. Consequently, this part of the workflow, especially when dealing with multi-phase tectonics, is often neglected and estimates of the regional paleo-tectonic stress are often loosely approximated.

We have therefore used a new generation paleo-stress analysis (Maerten et al., 2016) based on the boundary element method (BEM, Maerten et al., 2014), to reduce uncertainty in the tectonic stress characteristics that must be used as boundary conditions in the geomechanical stress simulations described earlier. The method uses fracture data to recover the paleo-tectonic stresses through thousands of simulations, covering the range of all possible tectonic stress configurations. Then, for each simulation, it compares attributes of the modeled stresses with the observed fracture geometry. Finally, the simulations that give the best fit with observed fracture data are selected. Maerten et al. (2016) provided with a detailed description of the technique.

To better visualize and analyze the results of one paleo-stress inversion, which consists of thousands of simulations, Lejri et al. (2015) introduced the tectonic stress domain, which is visualized on a 2D graph for which the x-axis is the stress ratio $\bar{R}$, and the y-axis is the orientation (θ) of the maximum horizontal stress relative to north. A point in the domain represents a single simulation; each simulation is colored according to the computed fit, which varies from 0 to 1, between observed fracture and local stress orientations (Fig. 11). As we often have numerous observed fractures, the color symbolizes the mean fit of all the fractures. For a given model, the inversion procedure will try to find the best solutions ($\bar{R}$, θ) by minimizing some objective functions. These will be highlighted in the tectonic stress domain with appropriate colors. The result of paleo-stress inversion is the optimum simulation (best fit), which includes the orientation and relative magnitude of the principal stresses as well as the stress regime (normal, wrench or reverse fault regime). A maximum fit below 50% is considered as unlikely, a maximum fit between 50% and 70% is considered as likely and a fit above 70% is considered as very likely.

Paleo-tectonic stress inversion simulations are then performed for all key geologic events derived from previous restoration process. For each event, restored structures (faults, horizons, and natural fractures) are used to constrain the Paleo-tectonic stress inversion simulations.

3.3.4.2. Paleo-stress modeling. The best far field stress inversion solutions are then used to constrain forward simulations for key tectonic events. These simulations provide the full paleo heterogeneous 3D stress field that in turns are used to derive the attributes (i.e. mechanical type, orientation, and spatial density trend) of fault related tectonic fractures that could have developed in the subsurface.

3.3.5. Discrete fracture modeling

The calculated fracture attributes computed for key geologic events

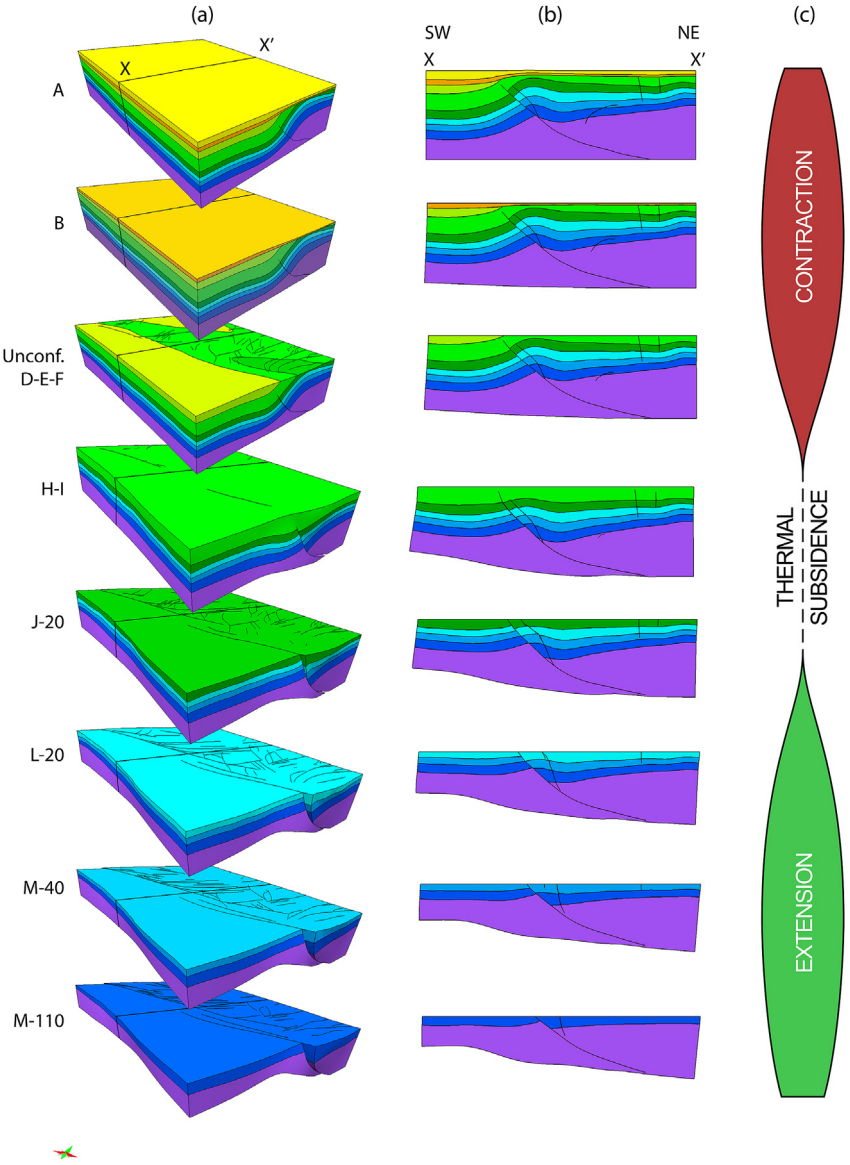

Fig. 9. Full restored sequence from Extension to contraction phases (section X-X′).

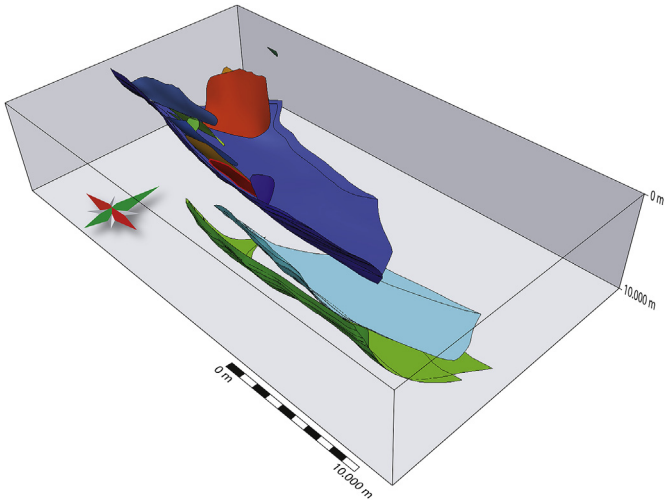

Fig. 10. Structural architecture of the restored fault framework corresponding to the extension tectonics.

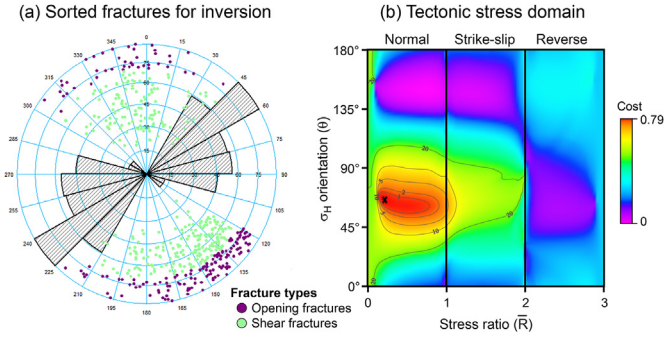

Fig. 11. First paleo-stress inversion results. (a) Stereonet with sorted fracture corresponding to the first phase of deformation. Rose diagram shows fracture strike and that the dots show dip. (b) Model simulated for the first step of the workflow for the Extension phase.

are then back transformed to the present-day 3D model configuration and used as drivers for constraining Discrete Fracture Network (DFN) simulations within the 3D reservoir grids. The fracture mechanical type and orientation derived from the computed stress tensor follow the

description defined earlier for the 3 fracture mechanical types (opening, closing or shearing). Regarding the density trend of these 3 fracture types, we follow Bourne and Willemse (2001) and Maerten et al. (2006).

3.3.5.1. Criterion for shear fractures. The potential for shear fractures to form can be estimated using the maximum Coulomb shear stress criterion (S_O). S_0 is the maximum shear stress acting on the two optimally oriented conjugate planes. A high value of S_O brings the Mohr circle closer to the shear failure envelope, such that the magnitude of S_O can be used as a proxy of shear fracture development. This assumption has been successfully used by Maerten et al. (2006) to model secondary normal faulting in a North Sea reservoir. The magnitude of S_O is defined as (Jaeger and Cook, 1979, p. 95):

$$S_0 = \tau_m(1/\cos\varphi) - \sigma_m.\tan\varphi \quad (2)$$

where $\tau_m = (\sigma_1 - \sigma_3)/2$ and $\sigma_m = (\sigma_1 + \sigma_3)/2$.

3.3.5.2. Criterion for opening fractures. The propensity for opening fractures to form should be related to the distance between the least compressive stress (σ_3) and the tensile failure envelop as low values of σ_3 brings the Mohr circle closer to the failure envelope. Therefore, we chose $\chi_{tensile}$ (Bourne and Willemse, 2001) as an index for joint intensity because it has been effectively used by Bourne et al. (2000) and Bergbauer and Maerten (2015) to model secondary jointing in several fractured reservoirs.

The value of the $\chi_{tensile}$ is determined by:

$$\chi_{tensile} = \tau_m - \sigma_m - C/2, \quad (3)$$

where C is cohesion. $\chi_{tensile}$ is equals to -σ_3 when there is no cohesion ($C = 0$).

3.3.5.3. Criterion for closing fractures. Here we simply use the magnitude of σ_1 as a proxy for closing fractures intensity trend. Indeed, the tendency for closing fractures to form should be related to the distance between the maximum compressive stress (σ_1) and the compaction failure envelop.

The outputs of this process are used to constrain the DFN using a stochastic method. To create the DFN five main parameters are necessary: (i) the distribution of fractures, which allows to assess the fracture intensity, (ii) the geometries of fractures, which are length and shape, (iii) the orientation of fractures, based on their mean dip and mean azimuth values, (iv) the concentration, which gives the range in which the modeled fracture orientation can deviate from its initial modeled orientation and (v), the fracture aperture. Once all the parameters are set, the process can be run to create the DFN corresponding to a chosen fracture set and tectonic event. By following the fracture attributes derived from the previously modeled heterogeneous stress field, the DFN can be locally perturbed around faults exhibiting changes in orientation and density trend. All DFNs corresponding to each key tectonic event are then combined to produce a final DFN in the present-day structure configuration.

4. Fracture modeling in the Malay Basin

4.1. Malay Basin data interpretation and analysis

4.1.1. Seismic interpretation

To generate a structural model honoring the complexity of the structures of the Malay Basin, the faults and horizons have been carefully depicted from the 3D seismic reflection data and quality controlled. The good quality of the seismic reflection data clearly shows the structures of the area such as an inverted rift structure with a sedimentary thickening toward the fault and also highlights many smaller scale steeply dipping faults cutting the main horizons in the hanging-wall (Fig. 2).

The refined structural-based interpretation included 71 faults (Fig. 6) and 12 horizons that were picked above and below the so-called Middle Miocene Unconformity.

4.1.2. Fault network analysis

A detail analysis of the seismically observed faults characteristics reveals two sets of faults. The first cluster characterized by a dip angle of a mean value of 61° in the shallow part and gentler at depth. These faults extend to a depth of about 3700 m, where they end or link to a detachment zone. They are all sub-parallel to a main EW trend with a mean strike of N82.5° (green faults in Fig. 7). Thickening toward the fault in the hanging-wall followed by erosion of the younger sections is the evidence for reutilization of the faults (i.e. tectonic inversion). The second cluster is characterized by a pattern of conjugated faults in map view with two average trends (N35° and N155°) and an angle of 60° between the two conjugate sets (red faults in Fig. 7). They are sub-vertical faults with a mean dip angle of 77° and they are much shallower faults than the other cluster, with a mean depth of about −2000 m. Because most of these faults affect the sediments deposited during the tectonic Inversion (Figs. 2, 6 and 7), they postdate the phase of tectonic extension (Fig. 7c).

4.1.3. Natural fracture analysis

Three wells with natural fracture data using image log were interpreted –in a depth slice from 1300 to 3100 m. Fig. 4 and Table 2 summarize the characteristics of the observed natural fractures. Fig. 4 shows Schmidt's stereo-nets of fractures (lower hemisphere representation) and their corresponding rose diagrams (strike orientation) for each well, while Table 2 summarizes the different observed fracture sets as well as the depth interval along which fractures were interpreted for each well.

The fracture strike varies from well to well, suggesting a heterogeneous distribution of sets of fractures associated with varying spatial orientations. One notes that the mechanical fracture types have not been set to all each observed fracture during the well log interpretation, leading to a high rate of uncertainty for the modeling (Maerten et al., 2016). Indeed, the paleo-stress inversion process needs both the seismically observed faults, generating stress perturbations, and fracture data such as natural fracture characteristics observed along wells including the (x, y, z) location of the fracture, its dip azimuth, dip angle and, the mechanical type. Therefore, a mechanical fracture type, as defined in section 3.3.1, was assigned to the un-typed fractures to better perform the paleo-stress inversion process. For instance, the fractures sub-parallel to the bedding (i.e. 0° < angle to bedding < 30°) with

Table 2
Fracture characteristics per well.

Well	Fracture dip angle	Fracture strike	Fracture depth
Well A	30° ≤ dip ≤ 75°	Srike1: N75° (± 20°) Strike2: N135° (± 15°)	−2200 m ≤ depth ≤ −1500 m
Well B	45° ≤ dip ≤ 75°	Strike1: N80° (± 20°) Strike2: N160° (± 5°)	−2500 m ≤ depth ≤ −1300 m
Well C	45° ≤ dip ≤ 90°	Strike1: N40° (± 20°)	−3100 m ≤ depth ≤ −2500 m

opening and no evidence of offset in the image logs were set as opening mode fractures (i.e. joints). All fractures with no evidence of opening in the image logs and with high angle to the bedding (i.e. 30° < angle to bedding < 70°) were set as shear fractures (i.e. faults or shear bands). Finally, the remaining fractures were set as closing mode fractures (i.e. compaction bands).

4.2. Malay Basin structural model building

The data used to build the model were the fault model including the 71 interpreted faults, the main unconformity and the 12 horizons. The stratigraphic attribute function in the area of interest derived from the volume-based modeling is shown in Fig. 8a. This stratigraphic attribute visualizes two different sequences on either side of an erosion surface.

From these implicit attribute, iso-surfaces representing the horizons are extracted with naturally perfect contacts along discontinuity surfaces *i.e.*, both the fault surfaces and the erosion surface. From these reconstructed surfaces a suitable sealed model representing the actual subsurface structure is built (Fig. 8b and c).

For restoration purposes it is necessary to reconstruct the missing parts of the model above the erosion surface (unconformity). To overcome this issue, the same volume-based modeling technique has been applied by using the stratigraphic attribute above the unconformity in the structure footwall as an extrapolation constraint to the hanging-wall. Fig. 8d shows the 3D structural model with the extrapolated eroded sections.

4.3. Malay Basin subsurface paleo-geometry restoration

A 3D restoration has been performed to recover the paleo-geometry of the structure over geological time, which then will be used to constrain the inverse and forward paleo-stress simulations.

4.3.1. Restoration model setup

In the following 3D restoration process, a homogeneous and isotropic elastic behavior characterized by two constants, Poisson's ratio and Young's Modulus is assigned to each modeled geological unit. Table 3 describes the rock properties used in the study which comprise the Young's modulus, the Poisson's ratio, the density, the porosity and the compaction constant. It is important to note that the present-day rock properties values have been used except for the porosity, which is the estimated initial porosity after the deposition of the sediments using an exponential compaction curve.

The 3D volume restoration workflow consists on, from the most recent to the oldest, sequentially removing the sedimentary layers one by one and to constrain the top of the next older layer to flatten along a horizontal surface representing the upper surface of the earth. This horizontal, planar datum is used as best assumption but may not reflect the paleo-topography at the time of deposition. Each of the displaced nodes is constrained to stay on the target surface but is free to move in the plane of that surface. For each stage of the restoration, all the other nodes of the model, unless otherwise constrained, are free to move until the system converges to the equilibrium while uncompacting. Since the model is 3D, a plane strain deformation is not required and hence the model components can displace in any dimensions.

To simulate the flow behavior of the rock over million years, the state of stresses is released for each step of the restoration, therefore, the restored geometry only is used as input for the next sequential restoration increment.

The modeled faults can slip with no friction but are constrained to stay in mechanical contact, thus preventing any opening *or* overlap of fault walls. This configuration permits a degree of freedom in which the fault can translate, rotate and deform during the restoration. The modeled horizons are not allowed to slip (*e.g.*, bedding slip) during the restoration.

Table 4
Paleo-tectonic stress for the Extension event.

Inverted paleo-tectonic stress for Extension phase	
$\sigma_H = \sigma_2 = 0.22$	Regime: Normal
$\sigma_h = \sigma_3 = 0$	Stress ratio: 0.22
$\sigma_v = \sigma_1 = 1$	Fit: 79%
σ_H orientation: N66°	

4.3.2. Complete paleo-geometry sequence

Two 3D sealed models have been built to perform the complete restoration of the area. The first model represents the present-day structure with layers above and below the unconformity (Fig. 8b). The second model represents the structure prior the so-called Middle Miocene Unconformity within the eroded layers reconstructed above the unconformity (Fig. 8d). Fig. 9 presents the full restored sequence in 3D (Fig. 9a), along a centered cross-section perpendicular to the main structure axis (Fig. 9b) and the geodynamic phases accordingly (Fig. 9c).

The restoration results clearly highlight the transition between the two main tectonic phases. The reconstructed steps between M-110 and J-20 belong to the rifting phase (Extension phase) and show how the basin has been filled with sediments in the hanging wall of the main listric EW trending normal fault. Then, from the deposition of J-20 units, the tectonic Inversion started with a clear basin inversion along the same major listric fault. The restoration results also illustrate that after the erosion the contraction phase continue until the present day. It should be noted that a significant amount of left-lateral strike-slip is observed along the main faults as a direct result of the 3D geomechanically-based restoration, which is in agreement with the known strike-slip along the regional faults in the Western Malaysian Peninsula (see Fig. 1).

Table 3
Rock properties per modeled units used in the 3D restoration process.

Age	Units	Rock properties				
		Young's modulus [Pa]	Poisson's ratio	density [kg/m^3]	Depositional porosity %	Compaction constant [1/m]
Pliocene - recent	A	2.99 E+09	0.37	2230	22	0.3343
Upper Miocene	B	2.99 E+09	0.37	2230	22	0.3343
Unconformity						
Middle Miocene	D-E-F	2.99 E+09	0.37	2230	22	0.3343
Lower/Middle Miocene	H—I	2.99 E+09	0.37	2230	55	0.3343
Lower Miocene	J-20	2.99 E+09	0.37	2230	55	0.3343
Upper Oligocene	L-20	2.99 E+09	0.37	2280	20	0.363
Lower Oligocene	M-40	1.12 E+10	0.34	2490	10	0.4648
Lower Oligocene	M-110	2.46 E+10	0.25	2590	6	0.4648
Cretaceous and older	Basement	2.46 E+10	0.25	2590	6	0.4648

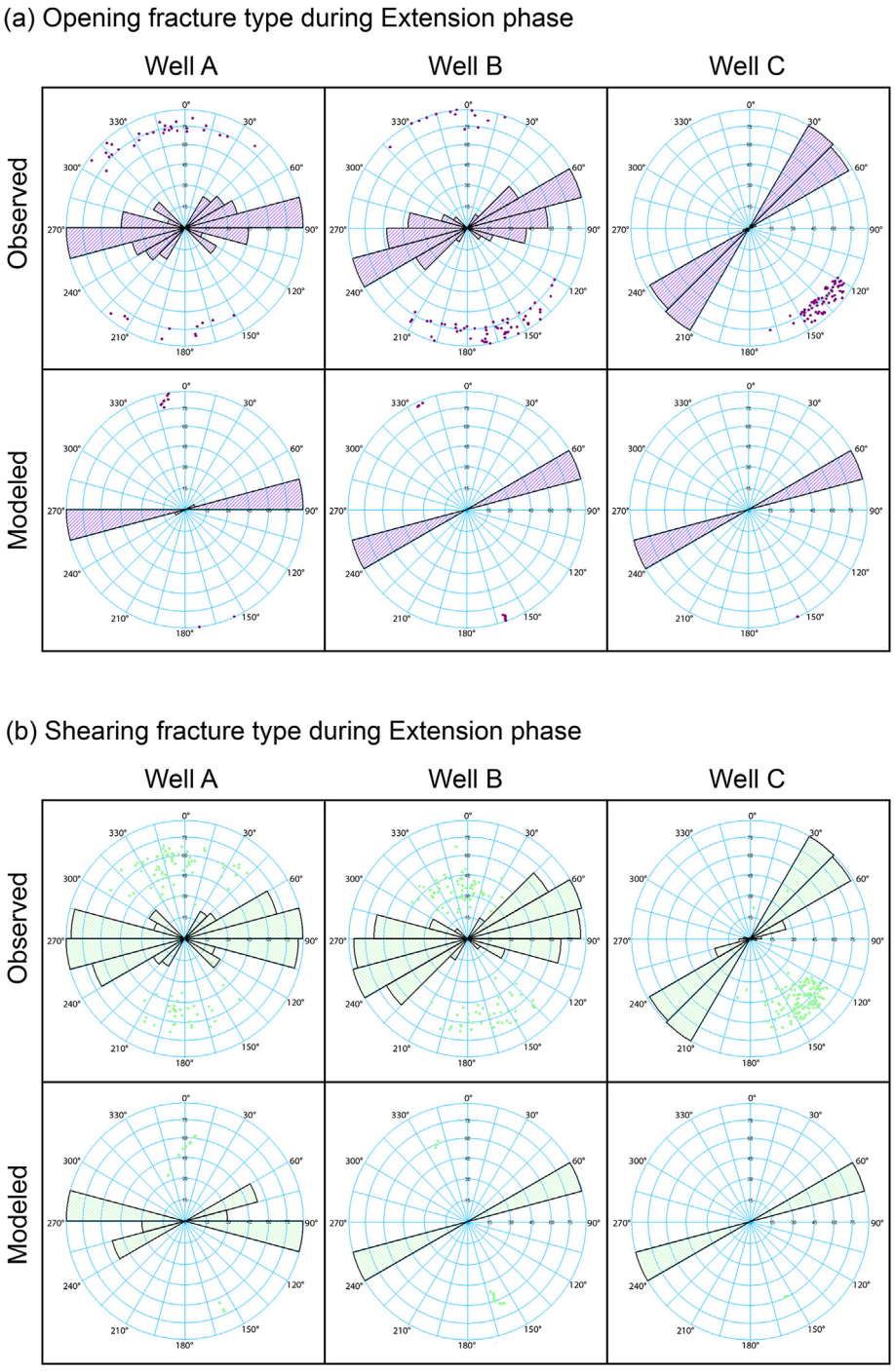

Fig. 12. Observed fractures versus modeled fractures. (a) Comparison of rose diagrams between observed and computed opening fracture type (joint). (b) Comparison of rose diagrams between observed and computed fractures type fault.

4.3.3. Key tectonic phases

The geological history of the Malay basin and the restoration results are consistent with two major tectonic events, which have occurred in the study area: a tectonic extension, from Paleogene followed by a positive tectonic inversion with a lateral component, from Neogene to present day. The characteristics of fractures at the time of their development depend on the local state of stress, which needs to be assessed for the two key phases of deformation. Therefore, the geological models used in the forward paleo-stress simulations should be representative of these two key geological events. For modeling the fracture related to the Extension phase, we decided to use the geometry at the end of the extensional phase, corresponding to time step J-20 (Fig. 9). Since the Contraction phase (positive tectonic inversion) is still active today, we made the decision to use the present-day geometry of the subsurface as the structural model for modeling the fracture related to the Inversion phase.

4.4. Malay Basin paleo-stress modeling

This step of the workflow comprises (i) the paleo-stress inversions to recover the far field paleo-stress tensors of the two previously defined tectonic phases and (ii), the forward geomechanical simulations of the same tectonic phases constrained by the inverted far field paleo-stress tensors. In all the following mechanical models we used a homogeneous

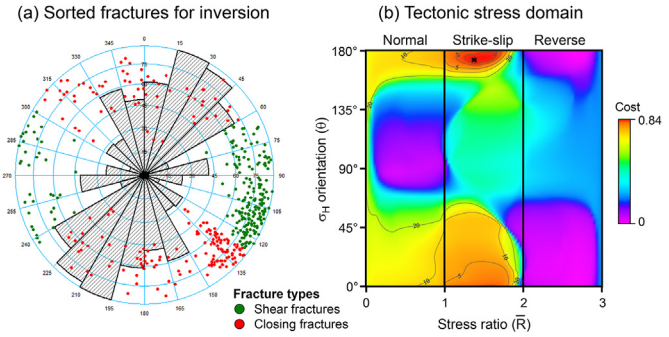

Fig. 13. Second paleo-stress inversion results. (a) Stereo-nets with two sets of sorted fracture corresponding to the tectonic inversion. (b) Tectonic model simulated for the third step of the workflow for the Inversion tectonics.

Table 5
Paleo-tectonic stress for the Contraction event.

Inverted paleo-tectonic stress for Inversion phase	
$\sigma_H = \sigma_1 = 1$	Regime: Strike-slip
$\sigma_h = \sigma_3 = 0$	Stress ratio: 1.38
$\sigma_v = \sigma_2 = 0.62$	Fit: 84%
σ_H orientation: N174°	

whole elastic space with a linear elastic and isotropic behavior characterized by two constants, Poisson's ratio and Young's Modulus. We used a value of 0.34 for Poisson's ratio (ν), 8 GPa for Young's Modulus (E), which are the mean values representative for the area of interest.

4.4.1. Extension tectonics

For this model step we intend to recover the characteristics of the Extension phase.. Faults assigned to the Inversion phase were removed from the model as they form latter while the Inversion phase was active (Fig. 10).

Fig. 11a shows a stereo-net (lower hemisphere representation) with restored fractures of the time-step J-20. To efficiently constrain the paleo-stress inversion, fractures with a strike ranging from N30° to N135° only were included in the simulation. A large spectrum of 105°, centered on the mean strike (N82.5°) of the seismic faults attributed to the Extension phase (Fig. 10), leaves a sufficient degree of freedom to the paleo-stress inversion to consider the perturbed stress field around the main active faults.. The mean strike (N52.5°) of all the fractures in the N30°-N135° windowis suggests that some of fractures are likely to have been developed within a perturbed stress field, considering the selected fractures as being induced by the Extension phase.

As described in the previous section Natural fracture analysis, fracture mechanical types were assigned to all fracture to better constrain the paleo-stress inversion (Fig. 11a).

The paleo-stress inversion using the selected and restored 3D faults model and the classified and restored fractures gives a normal fault regime where σ_H is oriented N66° (see Table 4), which is in good agreement with the expected ~ NS direction of extension for the Extension phase (Mansor et al., 2014). The cost of 0.79 on a scale from 0 to 1 for the best paleo-stress solution is considered as a good cost. Alternatively, the results are displayed in the tectonic stress domain of Fig. 11b, which also highlights the uncertainty in the value of the stress ratio within the normal fault regime.

From this best value of far field paleo-tectonic stress (see Table 4), the fracture set used for the inversion is sorted out such as each fracture owning a computed fit over 80% will be associated to the Extension phase and will not be used in the next paleo-stress inversion, which is meant to a second phase of deformation.

This best far field stress inversion solution is then used to constrain forward geomechanical simulation for the Extension phase. This simulation provides the full paleo heterogeneous 3D stress field that in turns is used to derive the attributes (i.e. mechanical type, orientation, and spatial density trend) of fault related fractures that could have developed during the Extension phase. To qualitatively check whether the far field paleo-tectonic stress found for the Extension phase is relevant, we compare the orientation of the observed fractures along the well with the modeled fractures derived from the computed stress tensor at the same xyz locations. The comparison is done in Fig. 12 for the two fracture mechanical types: (i) tension fractures, *i.e.* joints and (ii) shear fractures, *i.e.* faults or shear bands. It is shown that the fracture main trends are replicated including small variations for both fracture types.

4.4.2. Inversion tectonics

The fault model for the Inversion phase corresponds to the present-day geometry (Fig. 6) and all the interpreted faults are included in the model as initial fault attributed to the Extension phase could have been reactivated during Inversion phase.

Fig. 13a shows a stereo-net (lower hemisphere representation) of the remaining fractures that were not assigned to the Extension phase from the previous process. These fractures are represented in the present-day configuration.

As for the previous paleo-stress inversion, we assigned the missing mechanical fracture type to the remaining fractures that will be used to constrain this next paleo-stress inversion. We classified the fractures such that the fractures with a strike ranging from N150° to N220° are shear fractures, *i.e.* shear bands or faults and the fractures with a strike ranging from N40° to N150° are compression fractures, *i.e.* compaction bands. This classification is based on the image log observation, which helped define the mechanical type of most of the fractures and the results of several attempts, not exposed in this contribution, to classify the fractures with no clear observed mechanical type.

The paleo-stress inversion using the present-day 3D faults model and the remaining classified fractures gives a strike-slip fault regime where σ_H is oriented N174° (Table 5), which is in good agreement with the expected ~ NS direction of compression for the Inversion tectonics. The range of fitting values in the tectonic stress domain is between 15% for the lower fit and 84% for the best fit, which is considered again as very likely (above 70%). Alternatively, the results are displayed in the tectonic stress domain of Fig. 13b. From that best far field paleo-tectonic stress (Table 5), each fracture used for the paleo-stress inversion is sorted based on its own computed fit. All fractures with a fit between 80% and 100% will be associated to the Inversion tectonics. The remaining fractures that could not be associated to any of the two tectonic events, are considered as background fractures that could be explained by other mechanisms (i.e. folding, diagenesis, etc.) not investigated here. The remaining fractures represent only 15% of the total number of fractures.

As for the previous model, this best far field stress inversion solution is then used to constrain forward geomechanical simulation for the Inversion phase. This simulation provides the full paleo heterogeneous 3D stress field that in turns is used to derive the attributes of fault related fractures that could have developed during the Extension phase. We qualitatively check whether the paleo-tectonic stress found for the Inversion tectonics is relevant, by comparison of observed fractures orientations along the well with the modeled fractures orientations at the same location. The comparison has been done for the two fracture mechanical types: (i) compression fractures, i.e. compaction bands and (ii) shear fractures, *i.e.* faults or shear bands. Fig. 14 shows a good fit for each well, except for fracture type compaction band in the well A.

4.5. Malay Basin discrete fracture network modeling

As seen in the previous sections, the two main deformations, Paleogene Extension followed by the Neogene Contraction, described in Tables 4 and 5 and associated with their respective 3D fault models

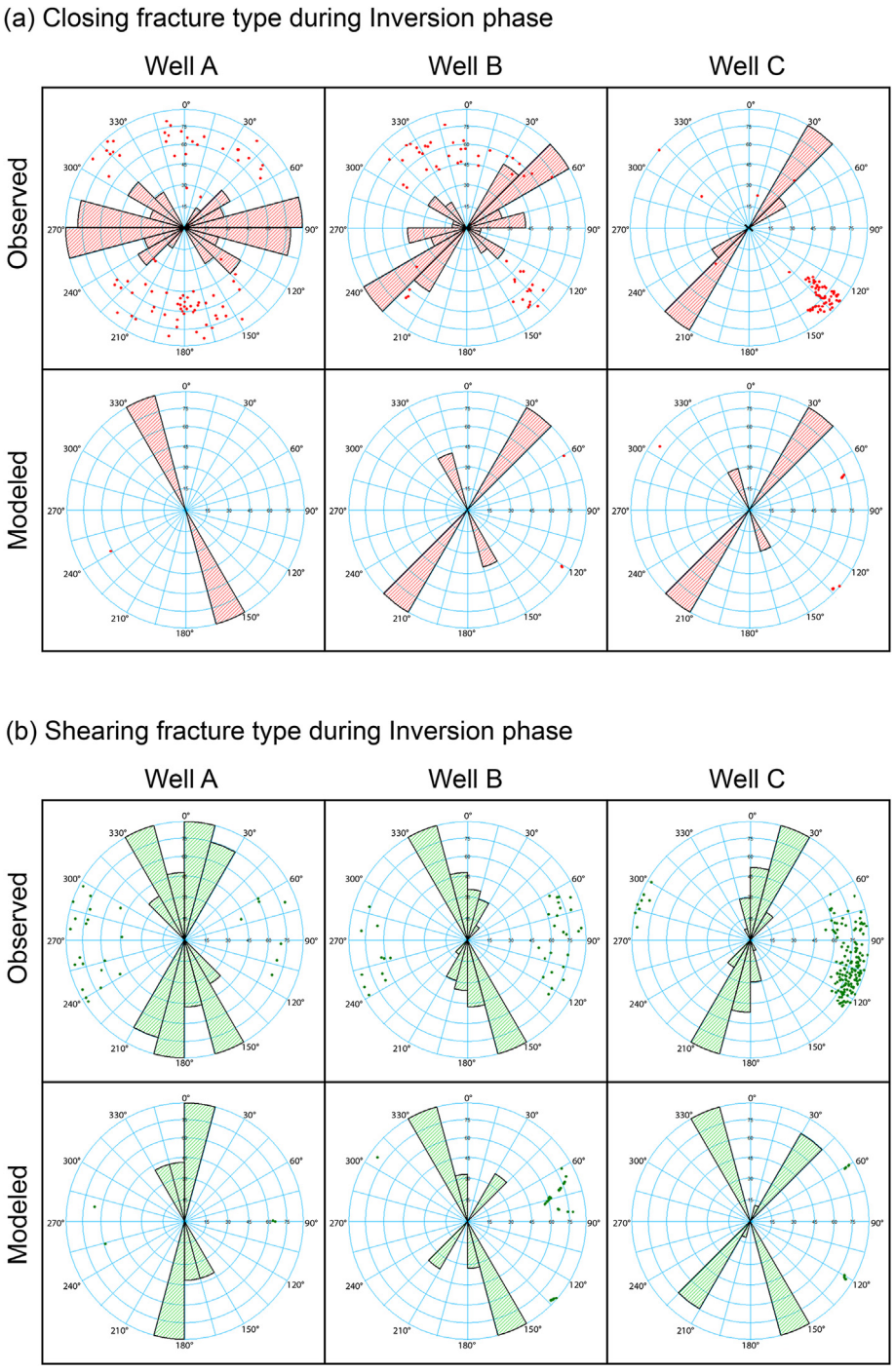

Fig. 14. Observed fractures versus modeled fractures. (a) Comparison of rose diagrams between observed and computed fractures type compaction band. (b) Comparison of rose diagrams between observed and computed fractures type fault.

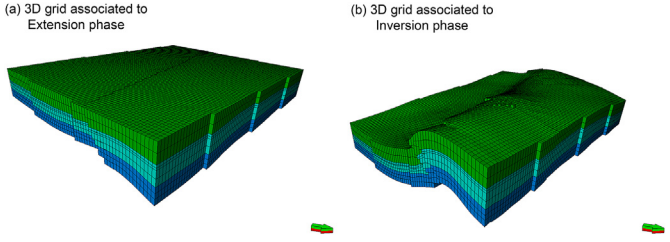

Fig. 15. 3D girds geometries for Extension tectonics (a) and contraction tectonics (b).

(Figs. 6 and 10), were used to constrain forward stress simulations around active faults that in turns will be used to drive the DFN modeling in the reservoir intervals.

For that purpose, we built two 3D grids including the reservoirs, with geometry constrained by the structural model of the corresponding two tectonic events (Fig. 15). At each cell of the 3D grids, the forward geomechanical simulations provide local stress tensors, which are used to generate (i) the fracture mechanical type (opening, closing or shearing), (ii) the fracture orientation (dip angle and dip azimuth) and (iii), the fracture density trend based on failure criteria, which should be as much as possible calibrated against the natural fracture density observed along wells when available. In the present study, the fracture

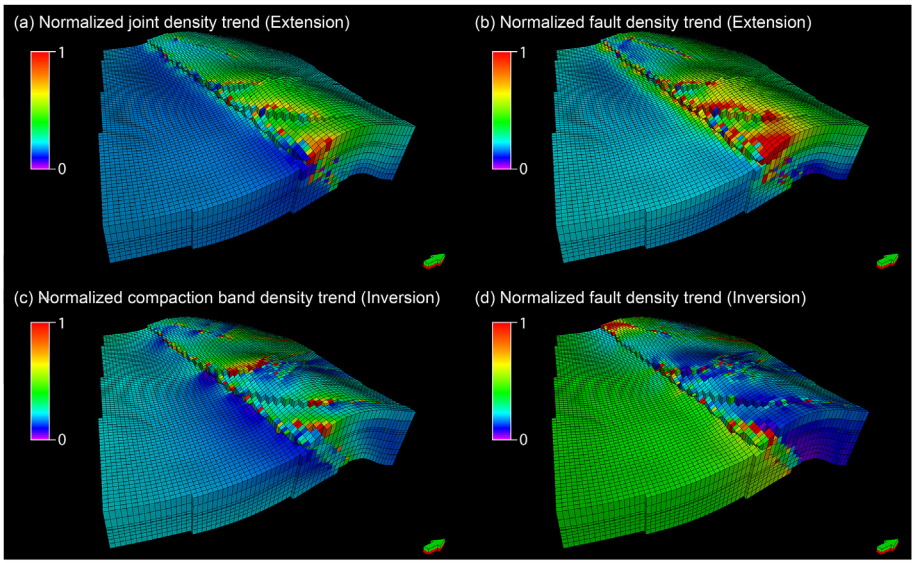

Fig. 16. (a) Normalized Intensity trend for opening fracture type (joints) during the Extension phase. (b) Normalized intensity trend for shear fracture type (faults) during the Extension phase. (c) Normalized Intensity trend for closing fractures type (compaction bands) during the Inversion phase. (d) Normalized Intensity trend for shear fracture type (faults) during the inversion phase.

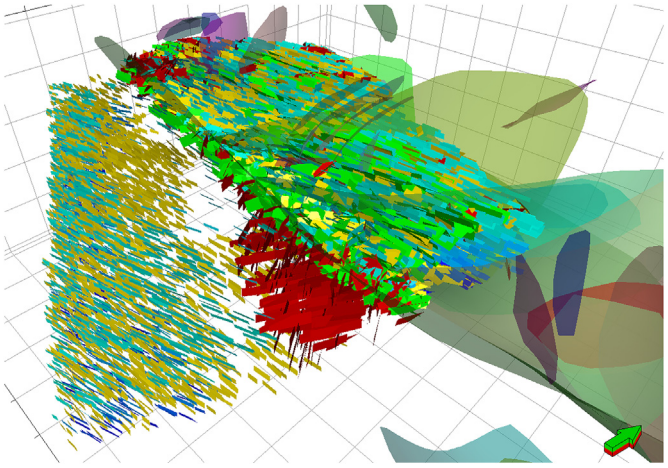

Fig. 17. Complete discrete fracture model with fractures from both tectonic events (Pre-inversion and syn-inversion phases) in present day geometries.

data observed on well logs and cores along the three wells were not continuous enough and incomplete, because of missing cores and heterogeneous quality of image logs, so no representative observed fracture density could be computed. Therefore, no comparison nor calibration of the modeled density trends against the natural fracture density observed along wells were possible. Nevertheless, the parameters (i.e. fracture type, orientation and density trend) derived from previous paleo-stress simulations are used to drive the DFN. All the other parameters necessary for modeling a DFN such as the fracture shape, size, concentration and aperture, are not described here as the primary focus of the present study is on the application of the proposed 4D geomechanical workflow for modeling natural fractures and not on the DFN simulation itself. Therefore, we only expend on the DFN generation and associated drivers that are produced by the previous modeling.

Based on the complete displacement field computed during the 3D restoration, the stress tensors modeled at each grid cell and use to derive the fracture orientation and intensity trends for the Extension tectonics, have been translated and rotated back to the present-day geometry. This process allows modeling a DFN corresponding to Extension phase in the present-day configuration. Fig. 16a and b show the normalized fracture intensity trends derived from the geomechanical model of the Extension event for the tension fractures (joints) and the shear fractures (small faults and/or shear bands) respectively. For both fracture types the highest intensity is mostly located in the hanging wall of the major listric fault and in the north-eastern part of the study area where the deformation is highest. Fracture intensity trend is also concentrated along the other major splay normal faults. Similarly, Fig. 16c and d show the normalized fracture intensity trends derived from the geomechanical model of the Inversion event for the closing fractures (compaction bands) and the shear fractures (small faults and/or shear bands) respectively. On one hand, closing fractures highest intensity values are in the hanging wall of the main thrust fault and distributed along the secondary sub-vertical conjugate faults active during the contractional deformation. On the other hand, shear fractures highest intensity values are in the footwall of the main thrust fault distributed along the active secondary sub-vertical conjugate faults of the hanging wall, especially in the western part of the study area.

As an illustration of the end product of the 4D geomechanical approach, Fig. 17 represents one DFN realization that combines the four fracture sets developed during the two tectonic events in the present-day 3D grid configuration. Only the large-scale fractures are represented as discrete fractures for this illustration.

5. Conclusions

We have shown that fault-related fractures in structurally complex reservoirs exposed to a multiphase tectonic history, such as in the Malay Basin, can be model using an innovative geomechanics-based 4D approach. The workflow consists of three main steps including, (i) the 3D restoration of the main structures which provides a good approximation of the geological model geometry for key tectonic events, (ii) the use of the paleo-geometry to constrain the simulations of the heterogeneous paleo-stresses over time and (iii), the analysis of the computed paleo-stress tensor that is used to understand the characteristics of the fault-related fractures that might have developed over time and that in turns are used to build a complete discrete fracture model in agreement with the tectonic events.

The application of this innovative approach to the Malay Basin confirms the evidence of two successive tectonic events: a Paleogene extension with a normal fault regime (σ_H = > N66°) and a Neogene contraction with a strike-slip fault regime (σ_H = > N174°), which lead to a positive tectonic inversion by the reactivation of inherited normal faults. Indeed, the modeling results agree with the known tectonic history of the area thought to be the consequence of the extrusion of Indochina (Tapponnier et al., 1982) coupled with the incipient collision of NW Shelf of Australia against Timor.

During these two main tectonic events, the stresses have been perturbed around the major active faults in terms of orientation and magnitudes, hence driving some of the natural fracture location and orientation during their growth. Most of the observed natural fractures along the three wells have been associated to the two main tectonic events. The remaining fractures, *i.e.* about 15% are either not related to faulting or inherited fractures.

Based on this positive correlation between computed stresses and observed fracture orientations, the stress distributions computed on the entire 3D reservoir grid for the 2 tectonic events have been used to derive the attributes (type, dip angle, dip azimuth and density trends) of the fault-related fractures. Even though the modeled fracture density trends could not be calibrated against the sporadically observed natural fractures along the wells, a complete model of discrete fracture network has been built in the present-day geometry of the reservoirs. This discrete fracture model is the combination of fractures developed during the Extensional deformation, such as joints and shear fractures and fractures developed during the Inversion tectonics, such as compaction bands and shear fractures.

These modeled fractures in the entire reservoir intervals can be used to define well trajectories whether to cross natural fractures of to avoid them. The proposed workflow improved the understanding of the fractured reservoir characterization and this is of help to appraise field development plans better.

Acknowledgements

PETRONAS is thanked for authorizing the publication of the case study from the Malay Basin as well as Schlumberger for the use of the software programs PETREL and Dynel3D, which comprise all the modeling technologies and processes used for the proposed workflow. We would like to thank also Dr. Mostfa Lejri for his help and support during this work. Finally, Dr. Peter Lovely and an anonymous reviewer are thanked for their constructive and thoughtful reviews.

Appendix A. Supplementary data

Supplementary data to this article can be found online at https://doi.org/10.1016/j.marpetgeo.2019.04.025.

References

Abul Khair, H., Cooke, D., Hand, M., 2013. Present-day in-situ stresses versus paleo-stresses for locating sweet spots in unconventional reservoirs. Australian Petrol. Product. Explor. Assoc. 53, 217–226.
Anderson, E.M., 1905. The dynamics of faulting. Trans. Edinb. Geol. Soc. 8 (3), 387–402.
Aydin, A., 1978. Small faults formed as deformation bands in sandstone. Pure Appl. Geophys. 116, 913–930.
Aydin, A., Borja, R.I., Eichhubl, P., 2006. Geological and mathematical framework for failure modes in granular rock. J. Struct. Geol. 28, 83–99.
Bergbauer, S., Maerten, L., 2015. Unlocking Stranded Resources in Naturally Fractured Reservoirs Using a Novel Approach to Structural Reconstructions and Palaeostress Field Modelling: an Example from the Hoton Field, Southern North Sea, UKCS. Geological Society, London, Special Publications, pp. 421.
Bourne, S.J., Rijkels, L., Stephenson, B.J., Willemse, E.J.M., 2000. Predictive modeling of naturally fractured reservoirs using geomechanics and flow simulation. GeoArabia 6, 27–42.
Bourne, S.J., Willemse, E.J.M., 2001. Elastic stress control on the pattern of tensile fracturing around a small fault network at Nash Point, UK. J. Struct. Geol. 23, 1753–1770.
Childs, C., Walsh, J.J., Watterson, J., 1990. A method for estimation of the density of fault displacements below the limits of seismic resolution in reservoir formations. In: In: Trotman, G. (Ed.), North Sea Oil and Gas Reservoirs, vol. 2 The Norwegian Institute of Technology, Liverpool.
Courrioux, G., Nullans, S., Guillen, A., Boissonnat, J.D., Repusseau, P., Renaud, X., Thibaut, M., 2001. 3D volumetric modelling of Cadomian terranes (Northern Brittany, France): an automatic method using Voronoï diagrams. Tectonophysics 331, 181–196.
Dahlstrom, D.D.A., 1969. Balanced cross sections. Can. J. Earth Sci. 6, 743–757.
Damsleth, E., Sangolt, V., Aamodt, G., 1998. Subseismic faults can seriously affect fluid flow - a stochastic modelling case study. SPE 49024, 1–11.
Dee, S.J., Yielding, G., Freeman, B., Healy, D., Kusznir, N.J., Grant, N., Andellis, P., 2007. Elastic dislocation modelling for prediction of small-scale fault and fracture network characteristics. In: In: Lonergan, L., Jolly, R.H., Rawnsley, K., Sanderson, D.J. (Eds.), Fractured Reservoirs, vol. 270. Geological Society of London, Special Publication, pp. 139–155.
Doust, H., Scott Sumner, H., 2007. Petroleum systems in rift basins-a collective approach in Southeast. Asian basins: Petrol. Geosci. 13, 127–144.
England, P., Molnar, P., 1990. Right-lateral shear and rotation as the explanation for strike-slip faulting in east Tibet. Nature 344, 140–142.
EPIC, 1994. Regional Study of the Malay Basin – Final Portfolios: Esso-PETRONAS Integrated Collaborative Study, Unpublished Report. Esso Production Malaysia Inc.
Fischer, M.P., Wilkerson, M.S., 2000. Predicting the orientation of joints from fold shape: results of pseudo-three-dimensional modelling and curvature analysis. Geology 28, 15–18.
Fletcher, R.C., Pollard, D.D., 1981. Anticrack model for pressure solution surfaces. Geology 9, 419–424.
Gauthier, B.D.M., Lake, S.D., 1993. Probabilistic modeling of faults below the limit of seismic resolution in Pelican Field. North Sea, offshore United Kingdom: AAPG (Am. Assoc. Pet. Geol.) Bull. 77, 761–776.
Gibbs, A.D., Jaffri, F., Murray, T., 1997. New techniques for fracture distribution and prediction from kinematic modelling of 3D strain fields. In: American Association of Petroleum Geologists Annual Convention Abstracts, vol. 40.
Hall, R., Morley, C.K., 2004. Sundaland Basins, vol. 149. American Geophysical Union, Washington D.C, pp. 5. https://doi.org/10.1029/149GM04.
Hamilton, W., 1979. Tectonics of the Indonesian Region. United States Geological Survey Professional Paper, pp. 1078.
Hennings, P.H., Olson, J.E., Thompson, L.B., 2000. Combining outcrop data and three-dimensional structural models to characterize fractured reservoirs: an example from Wyoming. AAPG (Am. Assoc. Pet. Geol.) Bull. 84, 830–849.
Hudson, J.A., 1981. Wave speeds and attenuation of elastic material containing cracks. Geophys. J. R. Astron. Soc. 64, 133–150.
Huchon, P., Le Pichon, X., Rangin, C., 1994. Indochina Peninsula and the collision of India and Eurasia. Geology 22, 27–30.
Hutchison, C.S., 1989. Geological Evolution of South-East Asia. Clarandon Press, Oxford, pp. 368.
Hutchison, C.S., 1992. The eocene unconformity on southeast and east Sundaland. Bull. Geol. Soc. Malays. 32, 89–108.
Hutchison, C.S., 2009. In: Tan, D.N.K. (Ed.), Geology of Peninsular Malaysia. University of Malaya/Geological Society of Malaysia, Kuala Lumpur 479 pp.
Jaeger, J.C., Cook, N.G., 1979. Fundamentals of Rock Mechanics. Chapman and Hall, London.
Jamison, W.R., 1997. Quantitative evaluation of fractures on Monkshood anticline, a detachment fold in the foothills of Western Canada. AAPG (Am. Assoc. Pet. Geol.) Bull. 81, 1110–1132.
Kingston, D.R., Dishroon, C.P., Williams, P.A., 1983. Global basin classification system. AAPG (Am. Assoc. Pet. Geol.) Bull. 67, 2175–2193.
Kloppenburg, A., Alzate, J.C., Charry, G.R., 2003. Building a discrete fracture network based on the deformation history: a case study from the Guaduas Field. In: Colombia: Extended Abstract for the VIII Simposio Bolivariano, Cartagena, Colombia.
Lajaunie, C., Courrioux, G., Manuel, L., 1997. Foliation fields and 3d cartography in geology: principles of a method based on potential interpolation. Math. Geol. 29, 571–584.
Lefranc, M., Mohamad-Hussein, A., Tan, C.P., Legand, X., Lee, B.C., Maerten, L., Press, D., Anis, L., 2014. Offshore Technology Conference Asia, 3D Structural restoration and Geomechanical Forward Modeling in a visco-plastic medium to natural fracture prediction in Malay producing field. In: Offshore Malaysia: Offshore Technology Conference, Kuala Lumpur, Malaysia, OTC-24753-MS.
Legrand, X., Joonnekindt, J.-P., Lee, B.C., Lefranc, M., Maerten, L., Anis, L., 2013. Innovative Natural Fracture Prediction Using a Geomechanically-Based Solution: Application to the Malay Basin (Malaysia). EAGE, Oman, pp. NFR13.
Lejri, M., Maerten, F., Maerten, L., Soliva, R., 2015. Paleostress inversion: a multi-parametric geomechanical evaluation of the Wallace-Bott assumptions. Tectonophysics 657, 129–143.
Lisle, R.J., 1994. Detection of zones of abnormal strains in structures using Gaussian curvature analysis. AAPG (Am. Assoc. Pet. Geol.) Bull. 78, 1811–1819.
Lovely, P.J., Flodin, E., Guzofski, C., Maerten, F., Pollard, D., 2012. Pitfalls among the promises of mechanics-based restoration: addressing implications of unphysical boundary conditions. J. Struct. Geol. 41, 47–63.
Madon, M., 1995. Tectonic Evolution of the Malay and Penyu Basins, Offshore Peninsular Malaysia. Ph.D. thesis. University of Oxford, UK.
Madon, M., 1997. The kinematics of extension and inversion in the Malay Basin, offshore Peninsular Malaysia. Bull. Geol. Soc. Malays. 41, 127–138.
Maerten, L., 1999. Mechanical Interaction of Intersecting Normal Faults: Theory, Field Examples and Applications. Ph.D. thesis. Stanford University, Stanford, California, U.S.A.
Maerten, L., Pollard, D.D., Gillespie, P., 2002. Effects of local stress perturbation on secondary fault development. J. Struct. Geol. 24, 145–153.
Maerten, L., Gillespie, P., Daniel, J.-M., 2006. 3-D geomechanical modeling for constraint of subseismic fault simulation. American Association of Petroleum Geologists 90, 1337–1358.
Maerten, L., Maerten, F., 2006. Chronologic modelling of faulted and fractured reservoirs using geomechanically based restoration: technique and industry applications. AAPG (Am. Assoc. Pet. Geol.) Bull. 90, 1201–1226.
Maerten, F., 2010. Geomechanics to Solve Geological Structure Issues: Forward, Inverse and Restoration Modeling. Ph.D. thesis. University of Montpellier II, Montpellier, France.
Maerten, F., Maerten, L., Pollard, D.D., 2014. iBem3D, a three-dimensional iterative boundary element method using angular dislocations for modeling geologic

structures. Comput. Geosci. 72, 1–17.
Maerten, L., Maerten, F., 2015. On a method for reducing interpretation uncertainty of poorly imaged seismic horizons and faults using geomechanically based restoration technique. Interpretation 3, 1–11.
Maerten, L., Maerten, F., Mostfa, L., Gillespie, P., 2016. Geomechanical paleostress inversion using fracture data. J. Struct. Geol. 89, 197–213.
Mallet, J.-L., 2002. Geomodeling. Oxford University Press, New York, NY, Applied Geostatistics.
Mansor, M.Y., Abd Rahman, A.H., Menier, D., Pubellier, M., 2014. Structural evolution of Malay basin, its link to Sunda block tectonics. Mar. Petrol. Geol. 58, 736–748. https://doi.org./10.1016/j.marpetgeo.2014.05.003.
Mollema, P.N., Antonellini, M.A., 1996. Compaction bands: a structural analog for anti-mode I cracks in aeolian sandstone. Tectonophysics 267, 209–228.
Moser, T.J., Howard, C.B., 2008. Diffraction imaging in depth. SPE 56, 627–641.
Munthe, K.L., Omre, H., Holden, L., Damsleth, E., Heffer, K., Olsen, T.S., Watterson, J., 1993. Subseismic faults in reservoir description and simulation. SPE 843–850 26500.
Murray, G.H., 1968. Quantitative fracture study-sanish pool, McKenzie county. In: North Dakota: American Association of Petroleum Geologists Bulletin, vol. 52. pp. 57–65.
Narr, W., Schechter, D.S., Thompson, L.B., 2006. Naturally Fractured Reservoir Characterization. Society of Petroleum Engineers 115 pp.
Neves, F.A., Zahrani, M.S., Bremkamp, S.W., 2004. Detection of Potential Fractures and Small Faults Using Seismic Attributes. The Leading Edge, pp. 903–906 September 2004.
PETRONAS, 1999. The Petroleum Geology and Resources of Malaysia. 665 pp.
Phillips, H., Joonnekindt, J.P., Maerten, L., 2014. Natural fracture prediction for discrete fracture modelling. In: 76th EAGE Conference and Exhibition, E103 01.
Polachan, S., Sattayarak, N., 1989. Strike-slips tectonics and the development of Tertiary basins in Thailand. In: Proceedings of the International Symposium on Intermontane Basins: Geology and Resources. Chiang Mai, Thailand, pp. 243–253.
Pollard, D.D., Aydin, A.A., 1988. Progress in understanding jointing over the past century. Geol. Soc. Am. Bull. 100, 1181–1204.
Sanders, C., Bonora, M., Kozlowski, E., Sylwan, C., 2002. From 2D to 4D Fracture Network Model, Structural Modeling of a Complex Thrust Trap: A Case Study from the Tarija Basin. SPE, Argentina, pp. 1–8 ISRM78184.
Sanders, C., Bonora, M., Richards, D., Kozlowski, E., Sylwan, C., Cohen, M., 2004. Kinematic Structural Restorations and Discrete Fracture Modeling of a Thrust Trap: a Case Study from the Tarija Basin, vol. 21. Marine and Petroleum Geology, Argentina, pp. 845–855.
Sassi, W., Livera, S.E., Caline, B.P.R., 1992. Reservoir compartmentalization by faults in cormorant block IV, U.K. In: In: Larsen, R.M. (Ed.), Structural and Tectonic Modeling and its Application to Petroleum Geology, vol. 1. pp. 147–156.
Schlische, R.W., Young, S.S., Ackermann, R.V., Gupta, A., 1996. Geometry and scaling relations of a population of very small rift-related normal faults. Geology 24, 683–686.
Schoenberg, M., Sayers, C.M., 1995. Seismic anisotropy of fractured rock. Geophysics 60, 204–211.
Schultz-Ela, D.D., Yeh, J., 1992. Predicting Fracture Permeability from Bed Curvature: 33rd U.S. Symposium on Rock Mechanics. pp. 579–589.
Stockmeyer, J.M., Shaw, J.H., Billingsley, L.T., Plesch, A., Wales, M., Lavin, L., Knox, R., Finger, L., 2018. Geomechanical Restoration as a Tool for Fractured Reservoir Characterization: Application to the Permian Basin, vol. 102. AAPG Bulletin, west Texas, pp. 103–128.
Sturzu, I., Popovici, A.M., Moser, T.J., Sudhakar, S., 2015. Diffraction imaging in fractured carbonates and unconventional shales. Interpretation 3, SF69–SF79.
Souche, L., Lepage, F., Iskenova, G., 2013. Volume based modeling - automated construction of complex structural models. In: 75th EAGE Conference & Exhibition Incorporating SPE EUROPEC.
Suppe, J., 1983. Geometry and kinematics of fault-bend folding. Am. J. Sci. 283, 684–721.
Tapponnier, P., Peltzer, G., Le Dain, A.Y., Armijo, R., Cobbold, P., 1982. Propagating extrusion tectonics in Asia: new insights from simple experiments with plasticine. Geology 10, 611.
Tapponnier, P., Peltzer, G., Armijo, R., 1986. In: From Coward, M.P., Ries, A.C. (Eds.), On the Mechanics of the Collision between India and Asia. 1986, Collision Tectonics, vol. 19. Geological Society Special Publication, pp. 115–157.
Thomas, A., Mallet, J.-L., De Beaucourt, F., 1974. Une Methode analytique de localisation des accidents structuraux dans un massif rocheux. In: Proceedings of the Congress of the International Society for Rock Mechanics, pp. 625–630.
Vidal-Royo, O., Cardozo, N., Muñoz, J.A., Hardy, S., Maerten, L., 2011. Multiple mechanisms driving detachment folding as deduced from 3D reconstruction and geomechanical restoration: the Pico del Águila anticline (External Sierras, Southern Pyrenees). Basin Res. 23, 1–19.
Walsh, J.J., Watterson, J., 1991. Geometric and kinematic coherence and scale effects in normal fault systems. In: In: Roberts, A.M., Yielding, G., Freeman, B. (Eds.), The Geometry of Normal Faults, vol. 56. Special Publication of the Geological Society, London, pp. 193–203.
Yielding, G., Walsh, J.J., Watterson, J., 1992. The prediction of small-scale faulting in reservoirs. First Break 10, 449–460.
Zahirovic, S., Seton, M., Müller, R.D., 2014. The cretaceous and cenozoic tectonic evolution of Southeast Asia. Solid Earth 5, 227–273.